Two-, three-, and four-particle exit channels in the reaction (806 MeV) Kr + U

P. A. Gottschalk* and G. Grawert

Kernphysik, Philipps-Universität, D-3550 Marburg, Federal Republic of Germany

P. Vater and R. Brandt

Kernchemie, Philipps-Universität, D-3550 Marburg, Federal Republic of Germany

(Received 31 January 1983)

Mica track detectors employing the 2π-geometry technique are used for coincidence measurements of multiple fragments in reactions induced by heavy ions. The nature of multiple fragment heavy ion induced reactions is shown to be binary from direct evidence. The process $^{84}Kr + {}^{nat}U$ at 9.6 MeV/u is studied as an example. Heavy fragments in the two-, three-, and four-particle exit channels are identified with respect to their masses and energies. Specific fragment-fragment correlations revealed the sequential nature of the reactions. Distributions of mass, energy, and angle are presented for the different reaction steps and the different exit channels.

NUCLEAR REACTIONS $^{238}U + {}^{84}Kr \rightarrow n$ heavy fragments, $E = 806$ MeV, measured tracks in mica, deduced mass-yield curves, energy and angular distributions.

I. INTRODUCTION

The phenomena of "deep-inelastic" processes are well established in reactions between heavy ions.[1] While for medium mass nuclei deep-inelastic processes are observed to have only modest cross sections, this reaction mechanism becomes increasingly important for heavier systems. With increasing mass of the colliding nuclei the nuclear interaction leads predominantly to three or more heavy reaction products in the exit channel.[2-4] For a detailed analysis of multiple fragment reactions the coincident spectroscopy of all heavy reaction products evolved from an individual interaction will be helpful and instructive. It is of interest, in particular, to study the initial interaction, if possible, and to obtain relative cross sections for exit channels with different numbers of outgoing (heavy) particles.

The reaction mechanism expected to account for most of the multibody events is the sequential process. In the first step, two primary fragments are formed after a quasi-elastic or deep-inelastic interaction and one or both subsequently fission as isolated nuclei. In the case of four or more (heavy) fragments in the final state a multiple sequential decay scheme might be appropriate where the event is the result of three or more distinct reaction steps. Alternative mechanisms could be instantaneous fission induced by Coulomb or nuclear forces,[5] multibody

breakup after fusion,[6] or fission and subsequent fusion.[7] All these multibody processes are distinctly different in their reaction pattern and one would expect different kinematical correlations between the coincident reaction products.

Complete correlation measurements provide direct information on the actual reaction mechanism and give further details of the dynamical process during the collisions.[8-11] For multibody processes, the large amount of independent kinematical variables as compared to only two outgoing particles make both experimental and theoretical investigations much more difficult and time consuming. However, recent work using electronic counter systems has overcome this difficulty and established proximity effects in heavy ion reactions with three outgoing particles.[11] This type of experiment is restricted to laboratories very well equipped with electronics.

The study of reaction products with mica or other solid state nuclear track detectors can be carried out in a wide variety of laboratories. The method is basically exclusive and not restricted to a small number of particles in the exit channel. It can be extended to fairly high numbers of particles in the exit channel—presently up to five fragments are observed in heavy-ion reactions.[4]

The passage of charged particles through mica produces radiation damage which becomes visible as tracks after etching. The existence of a threshold
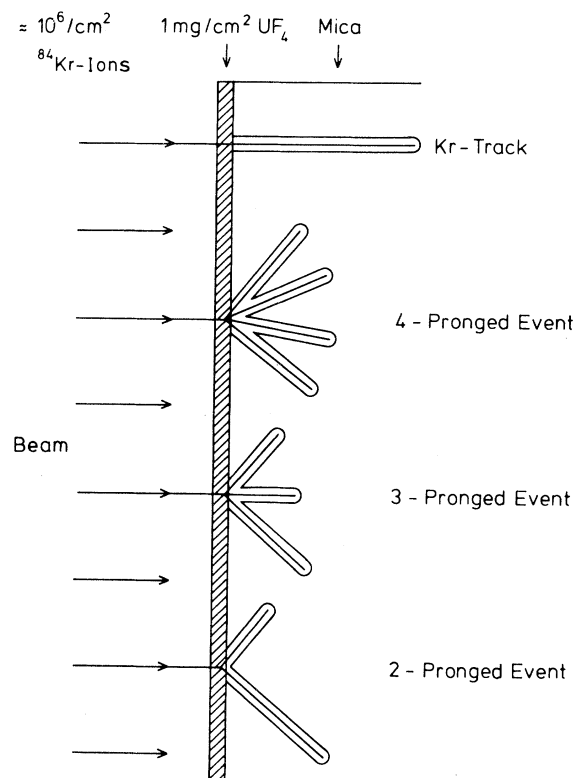
FIG. 1. Schematic representation of the 2π-geometry technique using mica track detectors. Also shown are sketches of typical events which are observed in this technique.

for the energy and the charge below which no observable track is recorded leads to a discrimination of heavy particles against a vast background of light particles also emitted during the collision.

Vater et al.[3] demonstrated the utility of mica track detectors for studying multifragment heavy ion collisions. Tracks have been scanned in three-dimensional space. A number of papers have been reported[12-14] which use similar techniques.

So far the interpretation of the track-detector data is based on qualitative arguments. Such data for multifragment heavy ion induced reactions have not been converted to masses and energies; quantitative and direct information on the actual reaction mechanism has not been extracted and the full scope of measuring track lengths and track directions has not been explored.

In the work reported here, the 2π-geometry technique using mica track detectors is investigated as a way to identify and study the reaction mechanism of multiple fragment heavy ion induced reactions. An effort is made to obtain spectroscopic information on the reaction products in reactions with up to four

heavy fragments in the exit channel. To this end a method for particle identification in the case of multibody exit channels will be presented. The method is based on a three-dimensional measurement of correlated tracks utilizing empirical velocity-range relations. Each track can be considered as a vector; its direction is determined geometrically, its length is to a first approximation a function only of the velocity of the penetrating particle.[15-17]

Fragment-fragment correlations are studied exploring the relationship between velocity, mass, and range and the additional information on the directions of the outgoing particles with respect to one another and to the beam. Direct evidence for sequential fission after quasi-elastic and deep-inelastic interactions is presented.

The paper presents detailed results for the reaction $^{84}\text{Kr} + {}^{nat}\text{U}$ at the incident energy of 806 MeV. Investigations following similar lines are given elsewhere.[4,18,19] Preliminary results were published previously.[20]

Section II summarizes the experimental technique. In Sec. III the method by which three-dimensional track data are converted into masses and energies is explained. Examples of the ability of the present method to reproduce known mass and energy distributions are given in Sec. IV. In the same section some discussion is devoted to a new empirical relationship between velocity, mass, and range which has been used throughout the present work. Section V contains the results, and, finally, summarizing remarks are presented in Sec. VI.

II. EXPERIMENTAL METHOD

The irradiation for the reaction

$$(806 \text{ MeV}) \ {}^{84}\text{Kr} + {}^{nat}\text{U} \rightarrow (n \text{ fragments})$$
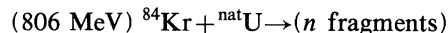
was carried out at the LINAC in Manchester. Also, for calibration purposes we irradiated ^{nat}U with ^{84}Kr in Orsay ($E_{lab} = 540$ MeV) and investigated track data from the reaction $^{nat}\text{U}(n_{th}, f)$.

The 2π-geometry technique as described in Ref. 2 was employed. Five sheets of freshly cleaved and cleaned mica of the muscovite type were annealed and covered with approximately 1.5 mg/cm² of UF_4 by vacuum deposition. These targets were irradiated normal to their surfaces by a low intensity beam. To obtain convenient track densities the exposure was restricted to approximately 2×10^6 particles/cm². After the irradiation the target layer was dissolved with HNO_3 and the mica was subsequently etched for 8 min in 48% H_2F_2 at room temperature. The etching conditions were chosen carefully so as to produce tracks equal in length to their etchable damage trails. After the irradiation no an-
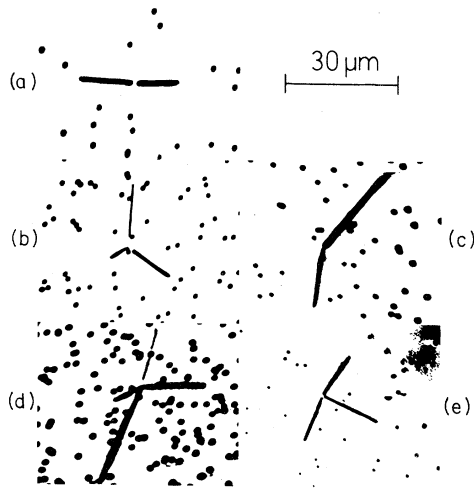
FIG. 2. Microphotographs showing tracks of projectiles (black dots) and (a) two-, (b) three-, and (d) four-pronged events, respectively, as seen in the plane perpendicular to the beam (forward hemisphere). Also shown are typical examples of "indirect" (c) three- and (e) four-pronged events. Here, at least one fragment for each multipronged event is scattered into the backward hemisphere, and is thus missing in the forward 2π geometry.

nealing procedures were employed. In this technique all heavy fragments with mass ≥ 30 u and scattered into the forward hemisphere ($\theta_{lab} \leq 85°$) are registered. Figure 1 gives a rough sketch of the experimental setup and the events which were observed.

As shown in Fig. 2, events due to nuclear collisions appear as multipronged events. Microphotographs of typical examples of two-, three-, and four-pronged events are shown for illustration purposes. Tracks of projectiles which penetrated the target without any interaction become visible as single spots if projected onto the plane perpendicular to the beam. By counting their number the heavy ion flux can easily be obtained,[21] allowing the determination of reaction cross sections.

Due to the 2π-geometry technique only those reaction products from an individual interaction which are scattered into the forward hemisphere of the laboratory system are registered. Fragments scattered into the backward direction are thus missing and, to some extent, the multiplicity of an event in the 4π-solid angle can only be estimated. Typical examples of these so-called "indirect" events are also shown in Figs. 2 (c) and (e).

A non-nuclear origin of tracks such as crystal defects can be excluded by optical inspection. The density of two-pronged events has been determined to be less than 10^{-1} events/mm^2. The accidental overlap of two independent two-pronged events resembling a four-pronged event is less than 10^{-4}, and is thus highly improbable on statistical grounds. Further reasoning, justified by direct evidence for excluding the latter explanation of the observed direct four-pronged event will be provided for in Sec. V B. In mica there is no directional dependence in the formation and developing efficiency of latent damage trails.[22]

The two-pronged events where one track enters the detector nearly normal to the surface are most difficult to recognize. These events correspond to elastically scattered fragments where the recoiling partner is to be found at $\theta_{lab} \geq 80°$ with a very short track. Most of the Rutherford cross section will thus presumably be suppressed due to technical limitations.

A total area of mica sheets of approximately 50 cm^2 was scanned directly under the microscope. Details about the numbers of registered events can be found in Table I (subset I). Whereas the quoted numbers of the (direct) three- and four-pronged events refer to the total area of 50 cm^2, only a limited portion of the scanned area was scanned for the two-pronged and the indirect three-pronged events. No event with a multiplicity higher than $n=4$ was observed in this work.

The three-dimensional coordinates of the tracks of coincidence reaction products were measured;

TABLE I. Numbers of multipronged events in (806 MeV) ^{84}Kr + ^{nat}U which have been observed, scanned, and used for the detailed spectroscopic analysis. Also indicated are the cross sections of the different exit channels. Subset I: registered events (total); subset II: scanned events; subset III: analyzed events.

Two-pronged			Indirect three-pronged			Three-pronged			Indirect four-pronged			four-pronged			Indirect + direct five-pronged
I	II	III	I	II	III	I	II	III	I	II	III	I	II	III	
496	206	178[a] +28[b]	347			149	131	110	4			1	1	1	No events
[b]$\sigma_2 \geq (150\pm35)$ mb			$\sigma_3 \leq (2235\pm340)$ mb						$\sigma_4 \geq (22.6\pm10.6)$ mb						$\sigma_5 \leq 20$ mb

[a]Elastic and quasi-elastic scattering.
[b]Deep-inelastic (TKEL > 120 MeV).

these constitute the data to be analyzed. Only randomly selected samples of the registered events have been measured in detail. Their numbers are given in Table I (subset II). In addition, 67 two-pronged events in the reaction 540 MeV ^{84}Kr + ^{nat}U (Ref. 2) and 108 two-pronged events originating from thermal-neutron induced fission of ^{nat}U were scanned for calibration purposes. The latter reaction was investigated using a 4π-geometry technique.[23]

The measurement of the lengths for individual tracks could be performed within ± 1.2 μm (standard deviation). Measured track lengths have been corrected for the passage through the target material. Spherical angles of individual tracks could be determined within $\pm 2.5°$ (standard deviation). The uncertainties include effects from range and angular straggling.

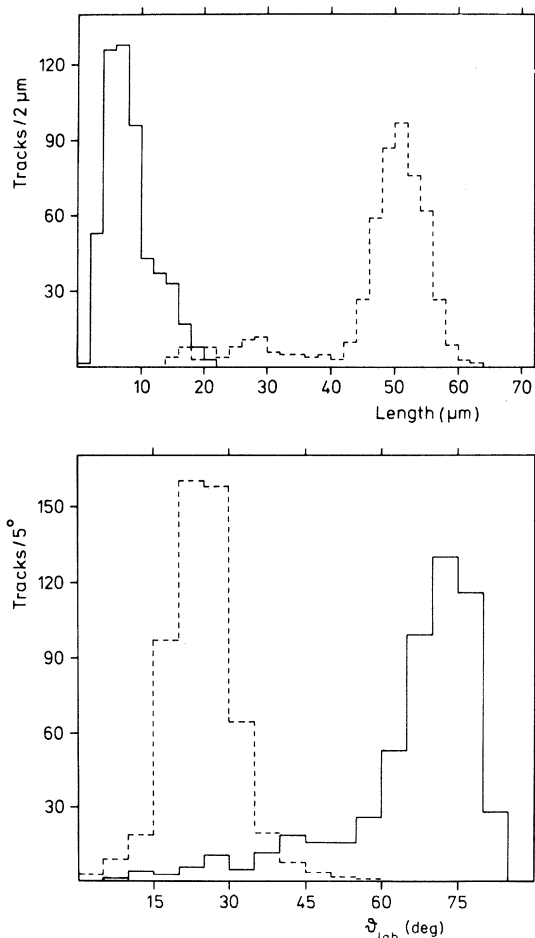The uncertainties quoted are typical for the bulk of the data, but do not hold for tracks at either very

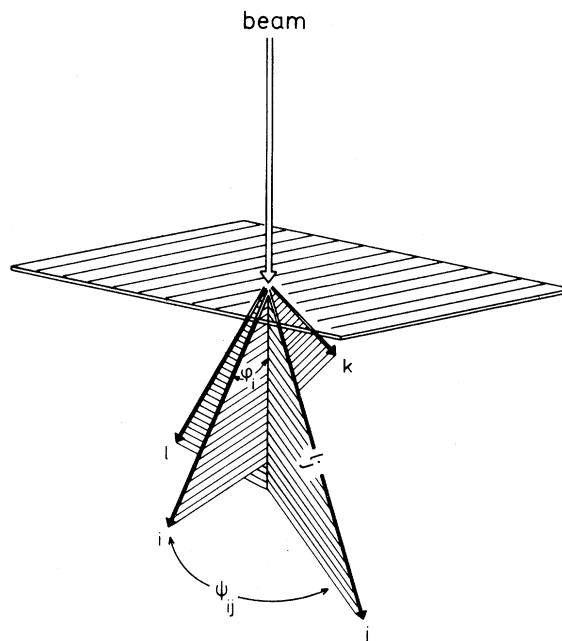

FIG. 4. Schematic representation of the four-pronged event [as shown in Fig. 2(d)] which has been observed and analyzed in (806 MeV) ^{84}Kr + ^{nat}U. (The spherical coordinates are listed in Table II.)

shallow or very steep angles. Also tracks which were found to have a final point within a track of an incident projectile could be measured only with lesser precision. Such events are registered and are taken into account only for the determination of cross sections.

As a typical example of directly measured values, we show in Fig. 3 for two-pronged events colinear in the plane of observation the track length distribution and the distribution of angles between the beam and tracks. One observes a fairly regular pattern: Two components are clearly distinguished, a short one and a long one, where the long one is scattered into the forward direction and the short one recoils around $\theta_{lab} \sim 80°$. Examples of directly measured values for three-pronged events are given in earlier references (i.e., Fig. 2, Ref. 3). The (direct) four-pronged event is shown in detail in Fig. 4 and Table II.

III. METHOD OF ANALYSIS

Each track is like a well-defined vector $\vec{l}_i$ in space and, correspondingly, each of the two-, three-, or four-pronged events is characterized by its correlated two, three, or four track vectors in the exit channel.

Assuming the conservation of momentum and mass, the correlated fragment masses m_i and veloci-

FIG. 3. Distribution of scattering angles (lab) and track lengths of correlated fragments in the two-body exit channel of ^{84}Kr + ^{nat}U at $E_{lab} = 806$ MeV. Note the experimental cutoff at forward angles.

TABLE II. Spherical coordinates of the four-pronged event which has been observed and analyzed in 806 MeV ^{84}Kr+^{nat}U (see Fig. 4).

l_i	l_j	l_k	l_l
14.2 μm	17.3 μm	29.1 μm	25.4 μm
ϕ_i	ϕ_j	ϕ_k	ϕ_l
79.9°	23.9°	55.5°	33°
ψ_{ij}	ψ_{jk}	ψ_{kl}	ψ_{li}
130°	40°	120°	70°

ties $\vec{v}_i$ from an individual multipronged event are calculated on the basis of the measured correlated track lengths l_i and track directions $\vec{e}_i$. For this purpose we solved event by event the coupled equations

$$\sum_i^N m_i V_i(l_i,m_i)\vec{e}_i = \vec{p}_{in} ,$$

$$\sum_i^N m_i = m_p + m_t , \tag{1}$$

where $\vec{p}_{in}$ denotes the incident (linear) momentum and m_p and m_t are the masses of the projectile and the target, respectively. $V(l,m)$ is an empirical velocity-range relation. N is the multiplicity of the event (e.g., $N=2,3$, or 4).

Obviously, there is no simple relationship between length and fragment mass of an individual track in a multiply-pronged event. The balance of momenta of all the fragments involved determines the mass which has to be associated with a given track of a given direction and length.

The solutions of Eqs. (1) can easily be obtained provided the relationship between range and velocity is independent of the mass of the nuclei. Solutions for the two-, three-, and four-pronged events based on this simplifying assumption can be found in Appendix A. However, in order to obtain a higher accuracy—in particular for large velocities which are involved in the present investigations—the dependence of range on mass or charge of the penetrating ion has to be taken into account.[16,24] The crucial question of the velocity-range relation will be discussed in Sec. IV A

For velocity-range relations which are explicitly dependent on mass, Eqs. (1) cannot be solved in a closer form. Rather, the equations reduce for two- and three-pronged events to uncoupled equations, whereas for four-pronged events they reduce to coupled equations in the unknown masses. The type of equation depends on the analytical structure of $V(l,m)$.

In the present paper we choose

$$V(l,m) = \sum_{\mu=0}^{2} \sum_{\nu=0}^{4} c_{\mu\nu}m^{\mu}l^{\nu} . \tag{2}$$

The coefficients $c_{\mu\nu}$ are given in Table III; they were obtained from an internal calibration as will be discussed below.

Equations (1) and (2) are solved by standard numerical methods. Substituting the resulting masses back into $V(l,m)$ the velocities are obtained in a second step. To this end, a computer program PRONGY was developed.

The algorithm as described above is strictly valid only for unperturbed kinematics. In heavy ion reactions a cascade of light particles is emitted from the highly excited reaction partners. The well-defined kinematical relations between the primary reaction products are disturbed in such a case. Concerning the loss of nucleons and the perturbed kinematics, two questions arise. Firstly, although the evaporation of nucleons changes mass and momentum, Eqs. (1) assume the conservation of these quantities. Secondly, track data refer to secondary reaction products, whereas the primary fragments are the quantities of interest.

In Appendix B it will be shown that the kinematical determination of fragment masses and energies by means of secondary velocities and the total (primary) momentum has the effect of determining the primary fragment mass spectrum in a very good approximation. The reasons are twofold: Firstly, the emission of light particles is isotropic in the fragment center-of-mass system. This feature has been verified in deep-inelastic collisions for the whole range of Q values from the relaxed events up to very small energy losses.[25] Secondly, there are only small, if any, differences in the range of primary and secondary fragments with different mass numbers but equal velocities. Primary masses and fragment masses which are kinematically deduced by

TABLE III. Coefficients of the empirical velocity-range relation in mica.

$$V(l,m) = \sum_{\mu=0}^{2} \sum_{\nu=0}^{4} c_{\mu\nu}m^{\mu}l^{\nu}(\text{fm}/10^{-23}\text{ s}) ,$$

where m is the mass number and l is the range (mg/cm^2). The applicability of this formula is restricted to $30 < m < 260$ and $0.5 < l/\text{mg cm}^{-2} < 22$.

	$\mu=0$	$\mu=1$	$\mu=2$
$\nu=0$	1.020×10^{-1}	-9.527×10^{-4}	2.651×10^{-6}
$\nu=1$	1.984×10^{-2}	9.395×10^{-5}	-4.315×10^{-7}
$\nu=2$	9.016×10^{-4}	1.846×10^{-5}	-4.409×10^{-8}
$\nu=3$	-4.529×10^{-5}	-2.782×10^{-6}	8.106×10^{-9}
$\nu=4$	-2.642×10^{-7}	8.475×10^{-8}	-2.517×10^{-10}

solving Eqs. (1) and (2) differ less than about 1% for a change of 10% in the former caused by light particle emission, as illustrated in Fig. 5. As shown in Fig. 5, this conclusion holds for the bulk of the data but not for the very short tracks with $R < 3$ mg/cm^2.

Although isotropic emission of light particles makes no essential change in the kinematical spectrometry of heavy reaction products, it introduces a broadening in the distribution of resulting masses and energies. The distributions are, however, subject to a very small inherent dispersion if *velocity* measurements are employed. In the case of thermal-neutron induced fission of ^{nat}U the dispersion in the fragment mass is $\sigma^2 = 0.3$ u^2 from the emission of one neutron, ignoring other sources of error. Furthermore, this dispersion decreases with the square of the velocities of the final (heavy) fragments. For the high velocities involved in the present reaction these inherent resolution widths remain negligible even if more (up to 20) light particles are emitted.

The uncertainties in the kinematical determination of masses and energies are essentially related to the energy-loss fluctuations (range straggling), to angular straggling, and to the uncertainties in the measurements of the three-dimensional coordinates of tracks. The angular straggling can directly be examinated by the colinarity of the two-pronged events in the c.m. system. The amount of angular straggling is comparable to or even slightly larger than the spread introduced in the angles by the uncertainty in determining the Cartesian coordinates of the tracks.[21] Due to the straggling effects, in particular, the present technique for particle identification is not a high precision technique.

IV. DATA REDUCTION

A. Calibration, velocity-range relations, and accuracy of the kinematical determination of masses and energies

The most crucial part of our investigations is the attempt to convert the observed track lengths l_i and track directions $\vec{e}_i$ of correlated multipronged events quantitatively into the masses and energies of the reaction products according to Eqs. (1) and (2). We choose the following *internal* calibration methods:

(1) In thermal-neutron induced fission of uranium, we know the resulting mass-yield curve and, in addition, the distribution of the total fission fragment energies versus mass split.

(2) In the reaction (806 MeV) $^{84}Kr + {}^{nat}U$, we know the masses and the total energies of two-pronged events due to elastic scattering.

(3) In addition, we look for colinear two-pronged

events due to elastic scattering in the reaction $^{84}Kr + {}^{nat}U$ at a slightly lower incident energy $E_{lab} = 540$ MeV.

(4) As will be shown in Appendix B, the kinematical determination of fragment masses and energies by means of Eqs. (1) and (2) has the effect of determining the primary fragment mass spectrum. Thus, we look for the conservation of total mass for the inelastic reactions in (806 MeV) $^{84}Kr + {}^{nat}U$.

For converting track data into masses and energies we start choosing a certain trial set of coefficients $c_{\mu\nu}$ for Eqs. (1) and (2). The mass and energy distributions obtained in this way depend critically on the choice of the $c_{\mu\nu}$. In different experiments a slightly different mica was used. Accordingly, the velocity ranges are slightly different. Any differences, however, could be traced back to differences in the densities of the micas resulting in identical velocity ranges and identical coefficients $c_{\mu\nu}$ if compared via their weight densities (mg cm^{-2}).

The calibration was performed searching for the best set of coefficients $c_{\mu\nu}$ for which the following items are reproduced:

(1) the light and heavy mass peak of the fission fragments in $^{nat}U(n_{th}, f)$ as well as the (mean) fragment energies;

(2) the elastic line (i.e., $Q = 0$ MeV) and the mass peak of the elastic group (i.e., $m = 84$ and 238 u) in (806 MeV) $^{84}Kr + {}^{nat}U$;

(3) the elastic line and the mass peaks of the elastically scattered particles in (540 MeV) $^{84}Kr + {}^{nat}U$;
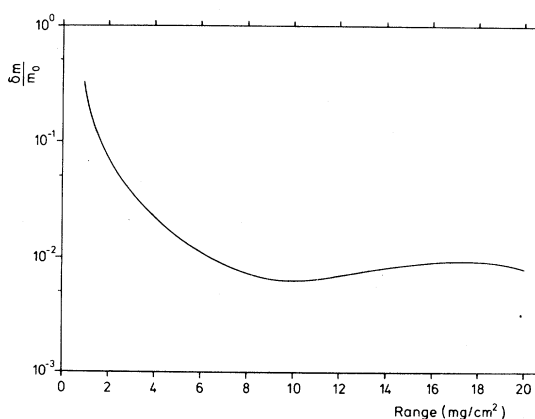

FIG. 5. The (mean) relative difference between the *primary* and the *computed* fragment masses versus the measured track lengths of the *secondary* fragments (see Appendix B). The parameters are as follows: primary mass $m_0 = 100$, secondary mass $m_2 = 90$, velocity-range relation according to Table III.
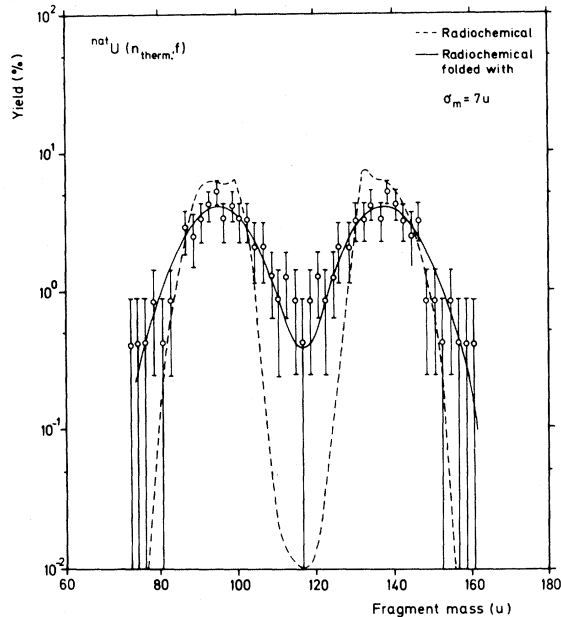
FIG. 6. Fission fragment mass yield curve for thermal neutron induced fission of ^{nat}U, obtained by a conversion of the track data based upon mass dependent velocity-range relation. The dashed line corresponds to radiochemical data. The solid line refers to the radiochemical data which are modified by the experimental uncertainty of this work ($\sigma_m = 7$ u).

(4) the total mass peak (i.e., $m = 322$ u) in the reactions

$$(806 \text{ MeV}) \; ^{84}\text{Kr} + ^{nat}\text{U} \rightarrow m_1 + m_2$$

$$\rightarrow m_1 + m_2 + m_3 \; .$$
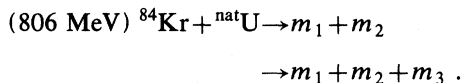
In Figs. 6—10 the results are presented. All these distributions have been obtained from our track data
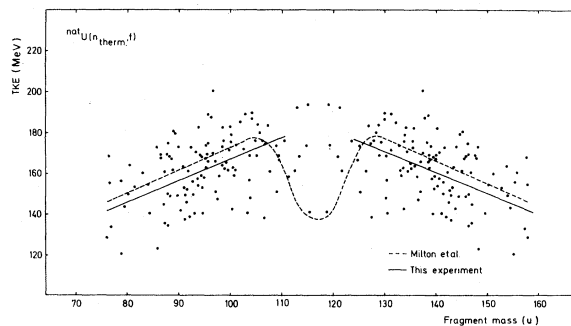

FIG. 7. Distribution of total fission fragment energies versus mass split. Conversion of track data is based upon the mass dependent velocity-range curve. The dashed line refers to counter experiments (Ref. 26), whereas the solid line is the regression line to the data assuming a linear dependence on the mass split.
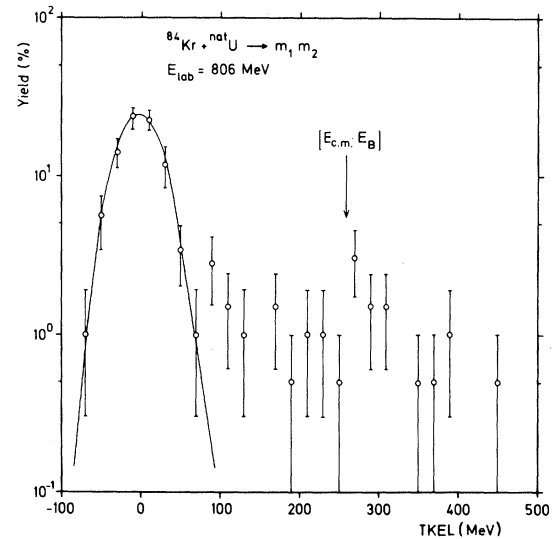

FIG. 8. Q values for the events displayed in Fig. 3. Also included are 67 two-pronged events from (540 MeV) ^{84}Kr + ^{nat}U. The solid line shows a Gaussian fit with $\sigma_E = 26$ MeV.

by the same set of coefficients $c_{\mu\nu}$. This "best" set of coefficients is given in Table III. Since our investigations are restricted to $30 < A < 260$ and $0.5 < l/(\text{mg cm}^{-2}) < 22$ the applicability of formula (2) and the coefficients $c_{\mu\nu}$ in Table III are restricted accordingly.

We now compare the actual distributions in our calibration data with the precise data. In Figs. 6 and 7 there are displayed the experimental mass yield and total fission fragment energy distributions as obtained by radiochemical methods and counter experiments[26] (dashed line) for thermal neutron induced fission of uranium. The solid line in Fig. 6 has been obtained by folding into the radiochemical data a mass resolution $\sigma_m = 7$ u. The solid line in Fig. 7 is the regression line assuming a linear dependence of the total fission fragment energy on the mass splitting. The mean fluctuation around this regression line equals $\sigma_E = 12.5$ MeV and is thus wider than the true width $\hat{\sigma}_E = 10.7$ MeV.[27] The relative errors in determining masses or energies correspond to 7% or 4%, respectively, in this most simple case (e.g., two-pronged events without momentum transfer).

In Fig. 8 the distribution of Q values for the two-pronged events in (806 MeV) ^{84}Kr + ^{nat}U is displayed. The elastically scattered events can clearly be identified by the peak around $Q = 0$ MeV. Quasi-elastic events are masked by the elastic component. Assuming that the width of the peak around $Q = 0$ MeV is essentially caused by the exper-
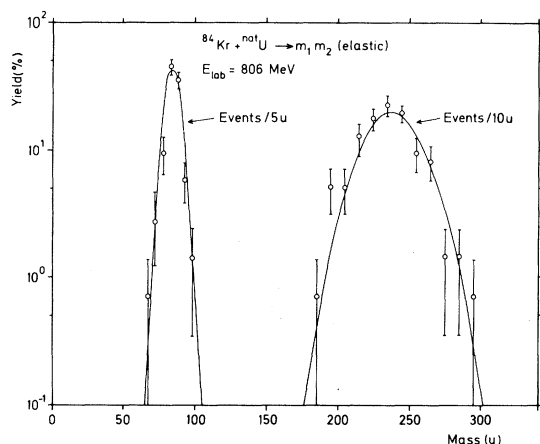
FIG. 9. Distribution of individual fragment masses of two-pronged events in $^{84}Kr + ^{nat}U$ (806 MeV) which are associated with elastic scattering. Also included are 67 two-pronged events from 540 MeV $^{84}Kr + ^{nat}U$. The experimental dispersion (Gaussian fits) are $\sigma_{m_L} = 6.4$ u and $\sigma_{m_H} = 19.3$ u.

imental uncertainty, we estimated the energy resolution to be $\sigma_E = 26$ MeV for the total kinetic energy of both fragments.

The distribution of masses of the elastic component (i.e., the data in Fig. 8 with $Q < 120$ MeV) is displayed in Fig. 9. Dominant peaks around $A = 238$ and 84 u are observed. The experimental uncertainties as obtained by a Gaussian fit to the data are $\sigma_{m,\text{light}} = 6.4$ u and $\sigma_{m,\text{heavy}} = 19.3$ u for the individu-
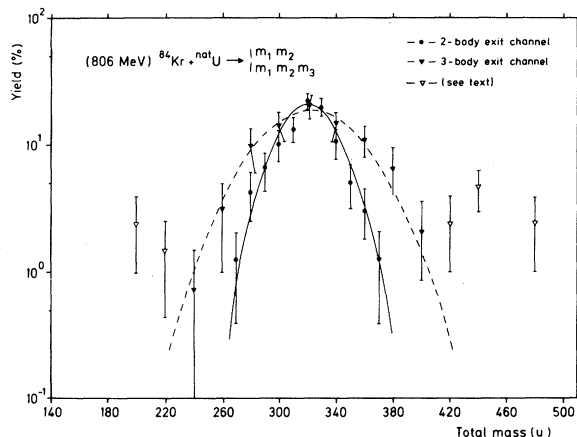

FIG. 10. Distributions of calculated total masses in the two- and three-body exit channels in (806 MeV) $^{84}Kr + ^{nat}U$. The solid and dashed lines refer to Gaussian fits with $\sigma_{2m} = 22$ u and $\sigma_{3m} = 34$ u, respectively. Also shown (open triangles) are the three-pronged events which have been registered but rejected in the subsequent detailed analysis (see Sec. IV C).

al masses. These widths can be taken as the resulting fragment mass errors for two-pronged events with momentum transfer. It should be noted that in Figs. 8 and 9 a total of 67 two-pronged events are included which have been observed in the reaction (540 MeV) $^{84}Kr + ^{nat}U$. The (relative) errors resemble the values which have been deduced in $^{nat}U(n_{th}, f)$.

As soon as the elastic peak around $Q = 0$ MeV and the light and heavy mass peaks of the elastic component are fixed by the coefficients $c_{\mu\nu}$ given in Table III, the widths σ_m and σ_E are stable with respect to slight changes in the $c_{\mu\nu}$. The quoted values of σ_m and σ_E thus reflect the true uncertainties in the kinematical determination of energies and masses by the present technique.

Since the second part of Eq. (1) is redundant for the three body exit channel and for the binary events with momentum transfer ($\vec{p}_{in} \neq 0$), the conservation of the total mass can be used as an independent test of the accuracy of the method or, vice versa, as an independent means for creating calibration lines. Distributions of total masses which are summed over all fragments in the two- and three-body exit channels are displayed in Fig. 10. A dominant peak is observed around the value, as expected from the conservation of total mass. As might have been anticipated from the higher numbers of degrees of freedom, the determination of mass in the three-body final channel could be performed only to a lesser precision as compared to the two-body channel. The ratio of the mean fluctuations, $\sigma_{3m}/\sigma_{2m} = 34/22$, is approximately equal to that of the square roots of the numbers of independent variables for the three- and two-body channel, respectively. In conclusion, for each degree of freedom, the relative experimental uncertainty in the determination of mass amounts to $\sim 3.5\%$.

In summary, by checking for the elastic lines and for the conservation of the total mass in the deep-inelastic region and by comparison with the fragment distributions in thermal-neutron induced fission of uranium, we achieved an internally consistent calibration valid for mica as stopping material and valid over the whole range of energies and masses which are of interest in the present investigation.

Calibration curves for some selected mass numbers are displayed in Fig. 11. They correspond to the empirical relationship between mass, velocity, and range as given in Table III. Also indicated in Fig. 11 are theoretical limits, $\hat{v}_{Kr}$ and $\hat{v}_U$, for the region of velocity-proportional stopping.[16] Furthermore, we give for comparison the theoretical velocity-range relation in mica for ^{138}Xe ions according to Northcliffe and Schilling.[24] For the
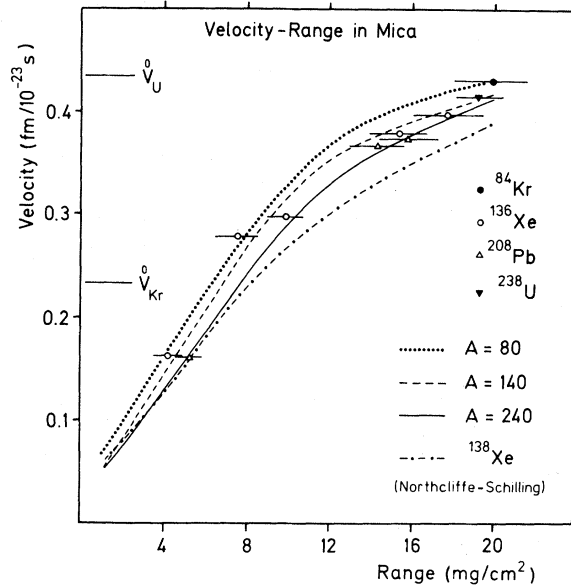
FIG. 11. Comparison of empirical velocity-range curves of this work for some selected nuclei with directly measured data of Ref. 20 and the predictions of Northcliffe et al. (Ref. 24) for ^{138}Xe. For the nuclei ^{84}Kr and ^{238}U there are also indicated the upper limits ($\hat{v}_{Kr}$ and $\hat{v}_U$, respectively) for the theoretically predicted region of velocity-proportional stopping (Ref. 16).

latter, Bragg's additivity rule relating the stopping power of a compound to its constituents has been employed.[28]

The overall agreement between our calibration curves and the curve of Northcliffe et al.[24] is reasonable provided the curves of Northcliffe et al. are corrected by an amount of about 20%. Similar conclusions, albeit for different stopping materials, have been noted elsewhere.[29] Furthermore, as can be judged by comparison with the theoretical limits, the region of velocity-proportional stopping is smaller than predicted. This is true, in particular, for the heavy mass region, i.e., for nuclei with mass $A > 140$ u.

Also shown in Fig. 11 are directly measured ranges of well-defined heavy ions.[20] These data agree with our calibration curves within their experimental uncertainties. It should be noted that the experimental uncertainties which are involved in the directly measured ranges are not identical to the uncertainties in the present investigations. Rather, it is expected that the consideration of *correlated* fragments and the use of conservation laws tend to reduce the uncertainty which would exist for consideration of a single fragment.[30]

One further possibility of obtaining information on the accuracy of the experimental mass and ener-

gy distributions is that the track-length uncertainty and the track-direction uncertainty are transformed directly into the uncertainties of mass numbers and energies. Such a type of transformation has been performed for the four-pronged event as follows: The errors in the experimental masses and energies have been deduced from a Monte Carlo simulation of the experimental errors of the track data. Varying the track lengths and track angles within the experimental uncertainties, "new" artificial events were created and analyzed by the same procedure, e.g., by solving Eqs. (1) and (2). The results are presented in Sec. V B.

B. Discrimination of events

Some three-pronged events give quite unreasonable results in the numerical analysis; the results have to be considered physically meaningless. For a total of 21 events out of 131 three-pronged events (see Table I, subsets II and III), the error in the computed total mass was significantly larger and far beyond two standard deviations, as shown in Fig. 10 (open triangles). These events are characterized by at least one very short track which was observed at angles $\theta_{lab} \geq 70°$. Very short tracks are associated with the largest (relative) error in the determination of the Cartesian coordinates. These tracks also suffer from the largest angular and range straggling and, furthermore, the algorithm determining primary masses by secondary quantities is questionable (see, e.g., Fig. 5). In the subsequent analysis all such events were rejected in which the mass summed over exit-channel heavy fragments differed from the conserved total mass by more than two standard deviations; i.e., we accepted events with $250 < A_{tot} < 400$.

Genuine two-pronged events must be colinear in the plane perpendicular to the beam. Incomplete but genuine three-pronged events caused by sequential fission in the reaction plane ("in-plane fission") where one fragment is scattered into the backward direction are also colinear and cannot be distinguished geometrically from genuine two-pronged colinear events. Since one fragment is missing in the forward 2π-solid angle, the balance of momenta is heavily disturbed and it is conceivable that the computed mass summed over the registered tracks is different from the conserved value. 113 colinear two-pronged events have been found where the sum of the fragment masses was significantly less than the masses of projectile and target. Computed mass and conserved mass differed by more than two standard deviations. Again, these two-pronged events with $A_{tot} < 270$ have been systematically rejected. We classified these 113 as "indirect three-pronged events."
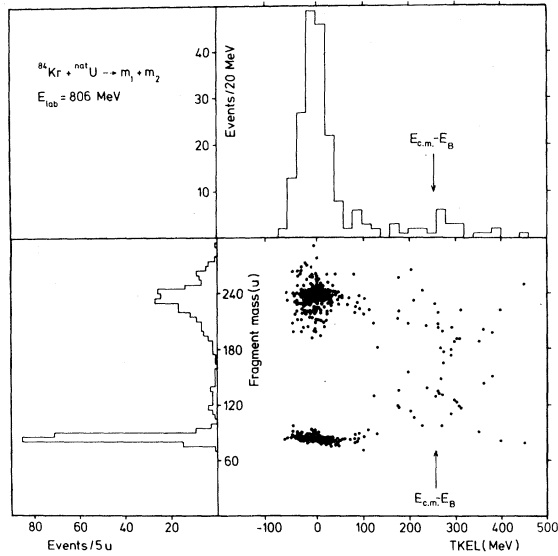
FIG. 12. Mass distribution of the two-body exit channel in (806 MeV) ^{84}Kr + ^{nat}U integrated over angles plotted versus the total kinetic energy loss. Indicated is the entrance channel Coulomb energy evaluated for two spheres at the distance equal to the interaction barrier. Only a small fraction ($\sim$20%) of the registered elastically and quasi-elastically scattered events is displayed. The data have not been corrected for the experimental uncertainty.

It should be stressed that the large amount of either "indirect" events or events with at least one very short track is caused by the unfavorable kinematical situation of the particular system (806 MeV) ^{84}Kr + ^{nat}U. Technical limitations caused by the restricted solid angle will become less important for systems with a stronger forward movement of the c.m. system, i.e., in studies of the system (U + U).[4]

V. RESULTS

A. Elastic scattering and total reaction cross section

In Fig. 12 the mass distribution, integrated over angles of the two body exit channel, is displayed as a function of the total kinetic energy loss (TKEL). Also indicated is the kinetic energy loss as obtained from the entrance channel Coulomb energy evaluated at a distance equal to the interaction barrier. Two well-defined components are clearly separated: the elastic or quasi-elastic events (TKEL < 120 MeV) with little or no mass transfer and the deep-inelastic component (TKEL > 120 MeV). Inelastically scattered projectiles and few nucleon transfer

products are masked by the elastic events. It should be noted that the data in Fig. 12 cannot be used as representative for cross sections since only a subset of registered events is displayed (see, e.g., Table I).

The angular distribution of the elastic component is shown in Fig. 13. The truncation at forward angles is biased due to our technique, whereas the deviation from the Rutherford cross section at larger angles results from the onset of nuclear reaction. The observed quarterpoint angle equals

$$(\text{lab})\theta_{1/4} = (35.3 \pm 1.8)^\circ . \tag{3}$$

Using this value and following the Fresnel scattering method of Frahn,[31] a theoretical total reaction cross section can be deduced

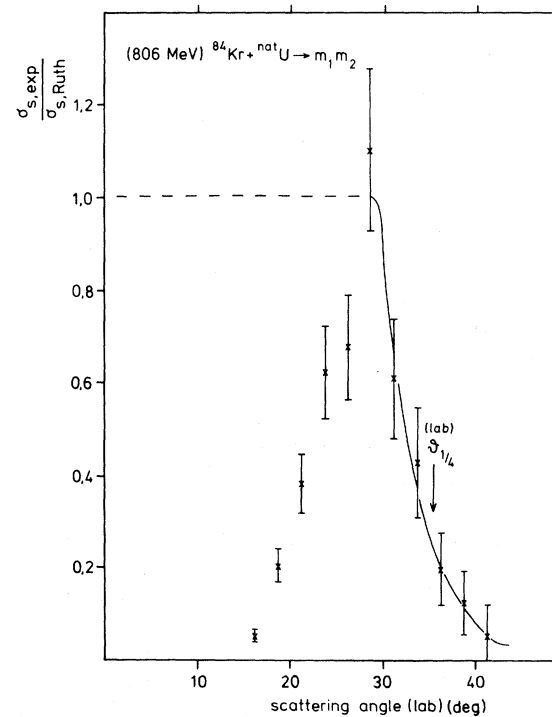$$(\text{th})\sigma_R = (2.7 \pm 0.3) \text{ b} . \tag{4}$$

FIG. 13. Ratios of the experimental scattering cross section to the Rutherford cross section as a function of the scattering angle (lab) in (806 MeV) ^{84}Kr+^{nat}U. The data correspond to the two-pronged events with TKEL < 120 MeV of Fig. 12. The truncation at forward angles is of technical origin. The quarterpoint angle is indicated. The solid line refers to a χ^2 fit (only data with scattering angles $\delta_{lab} > 27^\circ$ are taken into account). The ratio $\sigma_{exp}/\sigma_{Ruth}$ was assumed equal to unity at $\delta_{lab} < 27^\circ$ (dashed line).

The quoted uncertainties refer only to statistical errors, but might be larger to account for the errors due to inelastic products with little or no mass transfer.

The calculated value $(th)\sigma_R$ is in reasonable agreement with the observed total reaction cross section

$$(exp)\sigma_R = (2408 \pm 390) \text{ mb} , \qquad (5)$$

which has been obtained by counting all registered direct and indirect three- and four-pronged events and the deep-inelastic two-pronged events (see Table I). The close agreement shows that about 90% of all nuclear interactions are observed in the 2π geometry, as used in this work.

Various parameters of the Fresnel model which characterize the reaction (806 MeV) Kr + U are given in Table IV. The deduced interaction parameter $r_0 = 1.34$ fm agrees with values measured by other authors (see, e.g., the compilations in Refs. 1 and 32) for $Z_1 \cdot Z_2 \sim 3000$, Z_1 and Z_2 being the atomic numbers of projectile and target, respectively. Our value, however, is slightly smaller than that expected by Birkelund et al.[32] from a systematic analysis of several projectile-target combinations and the electron-half-density radii.

B. Four-pronged events

1. Cross section

One (direct) and four indirect four-pronged events have been observed. On the basis of these five events the cross section for the four-body exit channel equals

$$\sigma_4 \geq (22.4 \pm 10.6) \text{ mb} . \qquad (6)$$

Incomplete but genuine four-pronged events cannot be distinguished geometrically from three-pronged or two-pronged events. Genuine four-pronged events may thus be hidden among two- or three-pronged events. The above-mentioned value σ_4 should therefore be interpreted as a lower limit for the four-body cross section in the 4π geometry.

2. Indication for sequential fission

The tracks of the observed four-pronged event could be grouped pairwise (il) (jk) in correlated fragments with relative velocities.

$$v_{jk} = | \vec{v}_j - \vec{v}_k | = (0.182 \pm 0.011) \text{ fm}/10^{-23} \text{ s} , \qquad (7)$$

$$v_{il} = | \vec{v}_i - \vec{v}_l | = (0.253 \pm 0.009) \text{ fm}/10^{-23} \text{ s} . \qquad (8)$$

The alternative combinations resulted in very different values for the Galilean invariants v_{ik}, v_{jl}, v_{ij}, and v_{kl}. The correlated fragment pairs are arranged,

furthermore, in a way which excludes the possibility of an accidental overlap of two two-pronged events (see e.g., Fig. 4).

The quoted errors in v_{il} and v_{jk} were obtained by a Monte Carlo simulation, varying the input data—the track lengths and angles—within the experimental uncertainty of the track measurements, thus creating "new" and artificial four-pronged events. For each of these artificial events the "tracks" could be grouped in the same way: The correlations are not affected by the change in the input quantities.

For a sequential process we expect a fission Q value Q_{il}^f equivalent of that of a nucleus with mass $m_i + m_l$ and according to the following equation:

$$E_{il} = m_i m_l v_{il}^2 / 2(m_i + m_l) . \qquad (9)$$

The relative velocity v_{il} of fission fragments depends very weakly on the total mass and the fragment mass splitting of the fissioning system: The mean value of v_{il} for fission fragments varies within (0.24 ± 0.04) fm/10^{-23} s going from nuclei with mass $m_i + m_l = 140$ u up to $m_i + m_l = 300$ u and allowing for a mass ratio of $1 < m_i / m_l < 1.5$. The natural dispersion of v_{il} for a specific nucleus and fixed mass splitting falls well within the above limits. The same holds for the dependence on excitation energy $(E_x \leq 100$ MeV). In consequence, the kinematical correlations between the fragments of the four-pronged event as analyzed above suggest the sequential nature of this process.

We observed only one direct four-pronged event; the kinematical correlation between the fragments of the four-pronged event should not be overinterpreted. However, it is interesting to note that the results of the detailed analysis are also compatible with a sequential process and a decay chain as follows:

TABLE IV. Parameters of the reaction (806 MeV) ^{84}Kr + ^{nat}U which are deduced from the observed quarter-point angle according to the Fresnel scattering model of Frahn (Ref. 31).

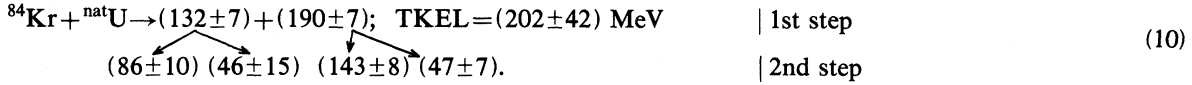| (lab)	(c.m.)
$\delta_{1/4} = (35.3 \pm 1.8)°$	$\theta_{1/4} = (47.0 \pm 2.3)°$
$\eta = 170.3$	
$k = 42.6$ fm^{-1}	$l_{max} = (392 \pm 21)$ h
$R_{int} = 14.03$ fm	$r_0^a = 1.34$ fm
$E_B^b = 340$ MeV	$\sigma_R = (2680 \pm 290)$ mb

^{a}Interaction radius parameter:

$$R_{int} = r_0 (A_1^{1/3} + A_2^{1/3}) .$$

^{b}Interaction barrier:

$$E_B = Z_1 Z_2 e^2 / R_{int} .$$

$$^{84}\text{Kr}+^{\text{nat}}\text{U}\rightarrow(132\pm7)+(190\pm7); \quad \text{TKEL}=(202\pm42)\ \text{MeV} \qquad |\ \text{1st step} \tag{10}$$

$$(86\pm10)\ (46\pm15)\quad(143\pm8)\ (47\pm7). \qquad\qquad |\ \text{2nd step}$$

The experimental fission Q values for the intermediate fragments agreed reasonably well with the values anticipated from ordinary fission:

$$Q_{132}^{\text{exp}}=(51\pm13)\ \text{MeV},\quad(Q_{132}^{\text{emp}}=68\ \text{MeV})\ ,$$
$$Q_{190}^{\text{exp}}=(118\pm12)\ \text{MeV},\quad(Q_{190}^{\text{emp}}=124\ \text{MeV})\ . \tag{11}$$

As before, the quoted errors were obtained by the Monte Carlo simulation. The artificial four-pronged events, introduced earlier, were analyzed using the present method. In Fig. 14 the distribution of prefission masses (the first reaction step of the artificial events) is shown as an example of the results obtained from this set of events. The width of the mass distribution is a measure of the accuracy of our method. It is of interest to note that the intermediate fragments of the first reaction step are formed after a large mass transfer and an appreciable loss of kinetic energy.

C. Three-pronged events

1. Cross section

Only a minor fraction of three-pronged events could be analyzed in detail (see Table I). The majority have been registered as "indirect" events. On the
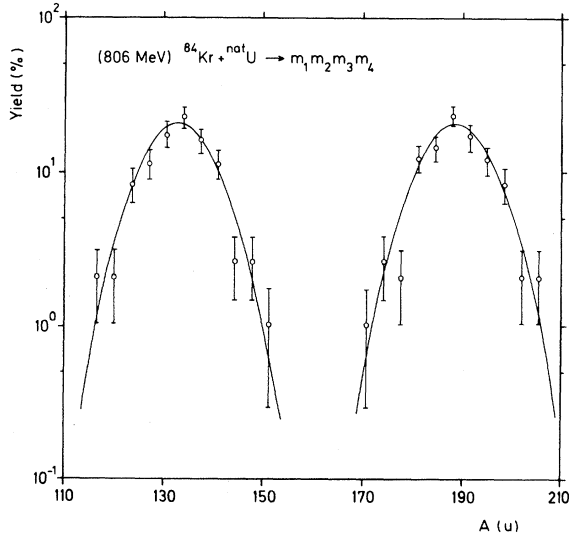
basis of the registered direct and indirect events the cross section for the three-particle exit channel has been calculated yielding

$$\sigma_3\le(2235\pm340)\ \text{mb}\ . \tag{12}$$

This reaction channel exhausts $\sim93\%$ of the total experimental cross section, demonstrating that ternary events are the major processes in the reaction $(806\ \text{MeV})\ ^{84}\text{Kr}+^{\text{nat}}\text{U}$.

2. Evidence for sequential fission

As before kinematical correlations have been found to yield direct evidence for the sequential nature of the three-particle exit channel. In Fig. 15 the distribution of velocity differences $v_{ij}=|\ \vec{v}_i-\vec{v}_j\ |$ is shown on an event-by-event basis. According to the combinatorial possibilities of grouping three particles into a pair (ij) and a spectator k, each event is represented in the histogram by three values. The subscripts i,j,k refer to the outgoing particles $(i,j,k=1,2,3;\ i\ne j\ne k)$. One peak is evident at
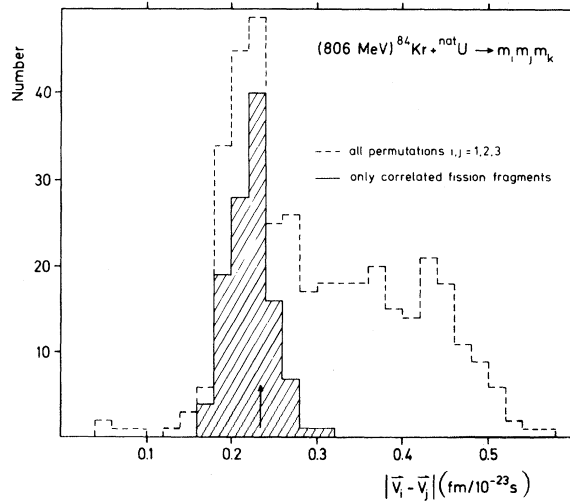

FIG. 14. Error in the prefission masses of the observed four-pronged event in $(806\ \text{MeV})\ ^{84}\text{Kr}+^{\text{nat}}\text{U}$ as obtained by a Monte Carlo simulation of the inaccuracy in the track-length and track-angle measurements.

FIG. 15. The distribution of the Galilean invariants $v_{ij}=|\ \vec{v}_i-\vec{v}_j\ |$ $(i,j=1,2,3)$ of the three-body exit channel in $(806\ \text{MeV})\ ^{84}\text{Kr}+^{\text{nat}}\text{U}$. The dashed histogram gives the result for all combinatorial possibilities of grouping three particles into a pair (ij) and a spectator k. For each three-pronged event at least one combination $(ij)k$ has been found where the velocity difference v_{ij} falls within the limits $(0.23\pm0.05)\ \text{fm}/10^{-23}$ s (solid line). Also indicated (arrow) is the most probable value $v_{ij}=0.23$ $\text{fm}/10^{-23}$ s.
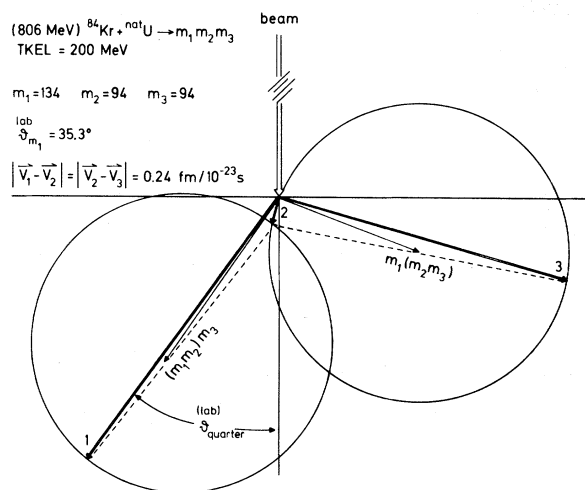
FIG. 16. Typical example for kinematical ambiguities in the Galilean invariants v_{ij}. Shown in the velocity diagram of a coplanar three-body final state which can be interpreted as originating from a deep inelastic collision (TKEL=200 MeV) followed sequentially by fission. Two possible sequential combinations arise: either scattering around the quarterpoint angle with large mass transfer and subsequent symmetric fission [i.e., Kr + U →134 + 188*→134 + (94 + 94)] or backward scattering (c.m. system) with little mass transfer and subsequent asymmetric fission [i.e., Kr + U→94 + 228* →94 + (134 + 94)].

v_{ij} =0.24 fm/10^{-23} s. This peak appears to be superimposed over a broad background tailing towards higher values. Actually, for each event at least one combination $(ij)k$ has been found where the velocity difference v_{ij} falls within the limits (0.23 ± 0.05) fm/10^{-23} s. The background results from the other two combinations.

The fact that not a single event was found which could not be grouped into a correlated fission fragment pair and an additional spectator strongly suggests the sequential pattern of the three-particle exit states. No broadening due to final state interactions has been found either. Rather, the width of the resonance in v_{ij} can be explained by the fluctuations in ordinary binary fission broadened additionally by the experimental resolution, particularly in some cases with unfavorable track geometries. On the average the error in determining the Galilean invariant v_{ij} equals Δv_{ij}=0.016 fm/10^{-23} s (standard deviation).

Kinematical ambiguities as sketched in Fig. 16 have been found in a subset of 42 (36%) events. The two possible sequential combinations differed significantly in the scattering angles (center-of-mass

system) corresponding to the first reaction step: One combination is associated with forward scattering of the projectilelike spectator at the quarterpoint angle (and backward scattering at $180°-\theta_{1/4}^{(c.m.)}$ of the intermediate system), whereas vice versa, the alternative combination results in backward scattering of the spectator and forward scattering of the prefission system. Events without kinematical ambiguities showed an angular distribution following a forward scattering of the projectilelike spectator. In the case of ambiguities in v_{ij} we assigned the sequential combination $(ij)k$ also to a forward scattering of the projectilelike spectator. The distribution of relative velocities of the correlated fragments which are obtained in this way is shown by the solid line in the histogram Fig. 15. It should be noted that here each three-pronged event is represented by one and only one value.

3. Mass distribution of the first reaction step

The distribution of the prefission masses is shown in Fig. 17. The light mass component and the complementary heavy mass branch peak at $A=78$ and 244, respectively. Prefission fragment masses equal to or even heavier than $A=280$ are artifacts. After correcting for the experimental resolution (light dashed line), a FWHM=24 u is estimated. Re-
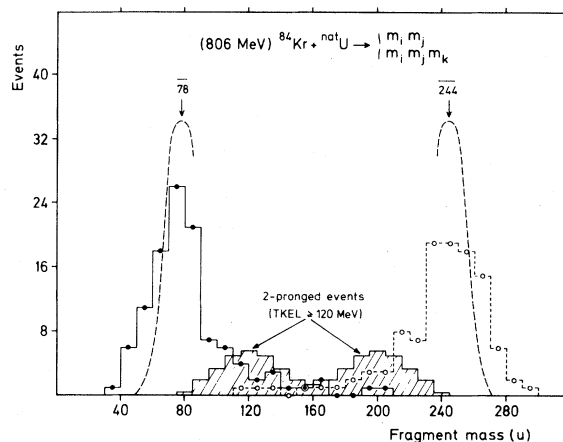

FIG. 17. Primary mass yield curve of the first reaction step in the three-body exit channel of (806 MeV) ^{84}Kr + ^{nat}U integrated over angles and energies. Prefission fragments and surviving reaction products are denoted by open and full dots, respectively. The light dashed curves refer to the distributions after corrections for the experimental uncertainties ($\Delta m/m \sim 8\%$). Also displayed by the hatched histogram is the mass distribution of the deep-inelastic component (TKEL > 120 MeV) in the two-body exit channel (after corrections). Note that only a fraction of the registered three-pronged events are displayed (see e.g., Table I, subset III).
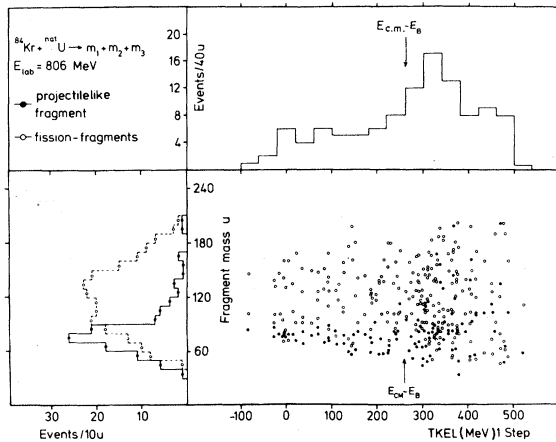
FIG. 18. Final mass distribution of the three-pronged events in (806 MeV) ^{84}Kr+^{nat}U integrated over angles as a function of the total kinetic energy loss (TKEL) in the first reaction step. Correlated fission fragment pairs are shown by open dots, whereas the uncorrelated spectator is referred to by the full dots. No corrections due to experimental uncertainties have been employed.

markably enough, large mass transfer can be observed tending towards symmetry. Even fragments around $A=160$ are obtained. As will be discussed below, no essential difference between prefission reaction products in the symmetric mass region in the three-particle exit channel and the deep-inelastic two-pronged events can be seen.

4. Distributions of masses and energies of the final fragments

In Fig. 18 the final mass distribution integrated over angles is displayed on an event-by-event basis as a function of the total kinetic energy loss (TKEL) of the first reaction step. Each three-pronged event is represented in this figure by three values: The uncorrelated spectator is shown by a full dot (or a full line in the mass spectrum), whereas the correlated fission fragment pair is indicated by a pair of open dots. No corrections due to experimental uncertainty have been employed.

A broad spectrum can be seen ranging from quasi-elastic to deep-inelastic events far beyond the entrance channel Coulomb energy. The interesting point is that the uncorrelated fragments are seen to be identical to the projectilelike fragments. We notice that with increasing energy dissipation the mass diffusion increases and that a remarkable shift towards symmetry occurs. Surviving fragments around a symmetric mass splitting can be seen associated with the largest energy loss. The overall fission fragment mass distribution appears to be nearly

symmetrical. A specific low energy cut (TKEL < 100 MeV) results in an asymmetric mass splitting.

D. Two-pronged events: Deep inelastic component

It is obvious that electronic counter experiments supplemented by radiochemical experiments[33] can study reactions with two particles in the exit channel considerably more accurately than the present mica technique. Therefore, we omit a detailed discussion of the deep-inelastic two-body exit channel in (806 MeV) ^{84}Kr + ^{nat}U. However, we would like to note the following gross features:

1. Cross section

Referring to Fig. 12 where two well-defined components are clearly separated, we define the deep-inelastic events to be those for which TKEL > 120 MeV. Actually, 28 deep-inelastic events in the two-body exit channel have been observed. On the basis of these events the total reaction cross section for the products that have survived a deep-inelastic collision without undergoing fission can be calculated as

$$(R)\sigma_2 \geq (150\pm35) \text{ mb} . \tag{13}$$

This value should be interpreted as a lower limit for the cross section in the 4π geometry for this particular reaction channel. It corresponds to $(5.8\pm1.2)\%$ of the observed total reaction cross section.

2. Distribution of masses and energies

No larger energy dissipation is observed for nuclei around and above the target nucleus (see e.g., Fig. 12), as might have been expected because of the enhanced fission probabilities of the heavy fragments. Rather, the deep-inelastic component is associated with a large mass transfer in the direction of symmetry. The heavy mass branch of the deep-inelastic component which survives fission connects continuously to the quasi-U branch which fissions sequentially. This feature is seen in the prefission mass distribution for the two- and three-pronged events as shown in Fig. 17.

VI. CONCLUDING REMARKS

In summary, a new and simple experimental technique has been investigated as a means of identifying and studying the reaction mechanism of multiple fragment heavy ion induced reactions. Spectrometric information on the reaction products in reactions with up to four heavy fragments in the exit channel has been obtained using mica track detec-

tors in the 2π-geometry technique. The (relative) mass resolution achieved amounts to $\sim 3.5\%$ per degree of freedom. Limitations of the investigated technique are due to low statistics, very forward scattering, and/or scattering into the backward hemisphere.

Final states with two, three, and four heavy fragments in the exit channel have been identified and analyzed. The sequential pattern of the multibody states has been verified by direct experimental evidence. The reaction (806 MeV) Kr + U is dominated by the sequential fission of the U-like fragments. Two- and four-body states are only minor reaction channels.

Large mass transfer has been observed which is directed towards symmetry. Fragments originating from such a transfer have been identified either as surviving fragments in the two-body or as primary reaction products in the three- and four-body channel. These are associated with an appreciable loss of kinetic energy.

ACKNOWLEDGMENTS

APPENDIX A: MASS-INDEPENDENT RELATIONSHIP BETWEEN VELOCITY AND RANGE AND THE KINEMATICAL DETERMINATION OF MASS

Assuming the conservation of incident momentum and total mass and neglecting any explicit dependence on mass in the relationship between range and velocity, the individual fragment for two-, three-, and four-pronged events can be obtained by solving Eqs. (1). The resolutions are given for the sake of completeness:

two-pronged events ($\vec{p}_{in} \neq 0$):

$$m_i = \frac{|\vec{p}_{in}|}{v_i \sin\psi_i (\cot\psi_i + \cot\psi_j)} \quad (i,j = 1,2) ; \tag{A1}$$

two-pronged events ($\vec{p}_{in} = 0$):

$$m_i = m_{tot} \frac{v_j}{v_i + v_j} \quad (i,j = 1,2) ; \tag{A2}$$

three-pronged events:

$$m_i = \frac{\vec{p}_{in}(\vec{e}_j \times \vec{e}_k)}{v_i \vec{e}_i (\vec{e}_j \times \vec{e}_k)} \quad (i,j,k = 1,2,3; \text{ cycl.}) ; \tag{A3}$$

four-pronged events:

$$m_i = \frac{(\vec{p}_{in} - m_{tot} v_4 \vec{e}_4)((v_j \vec{e}_j - v_4 \vec{e}_4) \times (v_k \vec{e}_k - v_4 \vec{e}_4))}{(v_i \vec{e}_i - v_4 \vec{e}_4)((v_j \vec{e}_j - v_4 \vec{e}_4) \times (v_k \vec{e}_k - v_4 \vec{e}_4))} \quad (i,j,k = 1,2,3; \text{ cycl.}) . \tag{A4}$$

Here, m_{tot} refers to the masses of the projectile and the target, $m_{tot} = m_p + m_t$, and v_i denotes the velocity corresponding to the length of the track due to the fragment labeled i, $v_i = V(l_i)$. The incident momentum is denoted by $\vec{p}_{in}$, and ψ_i and ψ_j are the scattering angles of the fragments i and j, respectively. The track directions (three-dimensional) are given by $\vec{e}_i$.

APPENDIX B: KINEMATICAL DETERMINATION OF FRAGMENT MASSES BY MASS DEPENDENT VELOCITY-RANGE RELATIONS AND THE INFLUENCE OF ISOTROPIC LIGHT PARTICLE EMISSION

Fragment velocities are essentially unchanged, on the average, by isotropic emission of light particles

in the fragment center-of-mass system. In the well-defined kinematical relations between the primary reaction products, the primary velocities can thus be replaced by the velocities of the secondary fragments

$$\sum_i m_{i0} V(l_i, m_{i2}) \vec{e}_i = \vec{p} ,$$

(B1)

$$\sum_i m_{i0} = m_{\text{tot}} .$$

Here, m_{i0} and m_{i2} refer to the masses of the primary and secondary fragments before and after the light particle emission, respectively. $\vec{e}_i$ is the (secondary) track direction and l_i is the observed (secondary) track length. The incident (primary) momentum is denoted by $\vec{p}$ and $V(l,m)$ is the relation between velocity and range which depends explicitly on the mass of the penetrating (secondary) fragments.

Again, the solutions of Eqs. (B1) are given by Eqs. (A1)–(A4), although here, the left- and right-hand sides refer to different masses. The algorithm as explained in Sec. III looks for a mass which is equal on both sides. This is the value m_i which satisfies the equation

$$m_{i0} V(l_i, m_{i2}) = m_i V(l_i, m_u) .$$

(B2)

Denoting the difference between the primary and the secondary mass by Δm and between the primary and the computed mass by δm, namely

$$\Delta m = m_{i0} - m_{i2} ,$$

$$\delta m = m_i - m_{i0} ,$$

(B3)

we find

$$\Delta m \left[-1 + \frac{\Delta m}{2m_0} \frac{m_0 V''}{V'} \right]$$

$$= \delta m \left[\frac{V}{m_0 V'} + 1 + \frac{\delta m}{m_0} \left[1 + \frac{1}{2} \frac{m_0 V''}{V'} \right] \right.$$

$$\left. + \frac{1}{2} \frac{\delta m^2}{m_0^2} \frac{m_0 V''}{V'} \right] .$$

(B4)

In Eq. (B4) we suppressed the index and denoted the partial derivatives of the velocity-range relation with respect to the mass (taken at the value m_0) by V', e.g.,

$$V' = \partial_m V(l,m) \,|\, m_0 .$$

Furthermore, we used the fact that $V(l,m)$ is almost quadratic in m [see Eq. (2) and Table III]. Equation (B4) expresses the difference between the primary mass and the computed mass in terms of m_0 and the relative mass change $\Delta m / m_0$. Up to second order in the relative mass change, the relative error in the computed mass is given by

$$\frac{\delta m}{m_0} = -\frac{1}{2} \frac{1+\epsilon}{\epsilon} (1 + \tfrac{1}{2}\eta)^{-1} \left\{ 1 - \left[1 - \frac{\Delta m}{m_0} \left[\frac{2\epsilon}{1+\epsilon} \right]^2 (1 \pm \tfrac{1}{2}\eta) \left[1 - \frac{\Delta m}{m_0} \eta \right] \right]^{1/2} \right\} ,$$

(B5)

where

$$\epsilon = \frac{m_0 V'}{V}$$

and

$$\eta = \frac{m_0 V''}{V'} .$$

Equation (B5) reduces in the first order in $\Delta m / m_0$ to the simple formula

$$\frac{\delta m}{m_0} = -\frac{\Delta m}{m_0} \frac{\epsilon}{1+\epsilon} .$$

(B6)

As can be seen, δm vanishes for $\partial_m V = 0$.

In reality, the velocity range relation is only slightly dependent on the mass of the penetrating fragment. For the relation Eq. (2) we find $\epsilon = 0(10^{-1})$. The quantity δm is thus smaller than Δm at least by an order of magnitude as demonstrated in Fig. 5. It is of interest to note that δm is a positive quantity. Kinematically deduced masses if calculated by the algorithm of Sec. III are therefore larger than the primary masses.

---

*Present address: Geschäftsstelle der Reaktorsicherheitskommission in der Gesellschaft für Reaktorsicherheit (GRS), D-5000 Köln, Federal Republic of Germany.

[1]R. Bass, Nuclear Reactions with Heavy Ions (Springer, Berlin, 1980).

[2]P. Vater, H.-J. Becker, R. Brandt, and H. Freiesleben, Nucl. Instrum. Methods 147, 271 (1977).

[3]P. Vater, H.-J. Becker, R. Brandt, and H. Freiesleben, Phys. Rev. Lett. 39, 594 (1977).

[4]P.-A. Gottschalk, P. Vater, H.-J. Becker, R. Brandt, G. Grawert, G. Fiedler, R. Haag, and T. Rautenberg, Phys. Rev. Lett. **42**, 359 (1979).

[5]V. Oberacker, H. Holm, and W. Scheid, Phys. Rev. C **10**, 1917 (1974).

[6]H. Diehl and W. Greiner, Nucl. Phys. **A229**, 29 (1974).

[7]H. H. Deubler and K. Dietrich, Phys. Lett. **62B**, 369 (1976).

[8]D. v. Harrach, P. Glässel, Y. Civelekoglu, R. Männer, and H. J. Specht, Phys. Rev. Lett. **42**, 1728 (1979).

[9]H. J. Specht, in *Proceedings of the International Conference on Nuclear Interactions, Canberra, Australia, 1978,* edited by B. A. Robson (Springer, Berlin, 1978), p. 1.

[10]P. Glässel, D. v. Harrach, Y. Civelekoglu, R. Männer, H. J. Specht, J. B. Wilhelmy, H. Freiesleben, and K. D. Hildenbrand, Phys. Rev. Lett. **43**, 1483 (1979).

[11]P. Glässel, D. v. Harrach, L. Grodzins, and H. J. Specht, Phys. Rev. Lett. **48**, 1089 (1982); D. v. Harrach, P. Glässel, L. Grodzins, S. S. Kapoor, and H. J. Specht, *ibid.* **48**, 1093 (1982).

[12]B. Grabez, Z. Todorović, and R. Antanasijević, in *Proceedings of the 10th International Conference on Solid State Nuclear Track Detectors, Lyon, 1979,* edited by H. Francois *et al.* (Pergamon, London, 1980), p. 899.

[13]M. Debeauvais, S. Jokic, and J. Tripier, in *Proceedings of the 10th International Conference on Solid State Nuclear Track Detectors, Lyon, 1979,* edited by H. Francois *et al.* (Pergamon, London, 1980), p. 927.

[14]G. Fiedler, R. Haag, J. Aschenbach, and T. Rautenberg, Gesellschaft für Schwerionenforschung, Darmstadt, Report GSI-J-1-77, 1977 (unpublished), p. 131.

[15]N. Bohr, K. Dan. Vidensk. Selsk. Mat.-Fys. Medd. **18**, no. 8 (1948).

[16]J. Lindhard, M. Scharff, H. E. Schiøtt, K. Dan. Vidensk. Selsk. Mat.-Fys. Medd. **33**, no. 14 (1963).

[17]L. C. Northcliffe, Annu. Rev. Nucl. Sci. **13**, 67 (1963).

[18]H. A. Khan, K. Rashid, R. A. Akber, G. Hussain, P. Vater, P.-A. Gottschalk, and R. Brandt, Nucl. Instrum. Methods **173**, 155 (1980).

[19]G. Fiedler, U. Steinhauser, T. Rautenberg, R. Haag, and P.-A. Gottschalk, Nucl. Instrum. Methods **173**, 85 (1980).

[20]R. Brandt, P.-A. Gottschalk, and P. Vater, Nucl. Instrum. Methods **173**, 111 (1980).

[21]P. Vater, dissertation, Philipps-Universität Marburg, 1976.

[22]H. A. Khan, G. Tress, P. Vater, and R. Brandt, Nucl. Tracks **4**, 109 (1980).

[23]P. Vater and R. Brandt, Radiochim. Acta **21**, 191 (1974).

[24]L. C. Northcliffe and R. F. Schilling, Nucl. Data Tables **A7**, 233 (1970).

[25]B. Tamain, R. Chechik, H. Fuchs, F. Hanappe, M. Morjean, C. Ngô, J. Péter, M. Dakowski, B. Lucas, C. Mazur, M. Ribrag, and C. Signarbieux, Nucl. Phys. **A330**, 253 (1979).

[26]J. C. D. Milton and J. S. Fraser, Can. J. Phys. **40**, 1626 (1962).

[27]M. Asghar, F. Caitucoli, P. Perrin, and C. Wagemans, Nucl. Phys. **A311**, 205 (1978).

[28]C. A. Sautter and E. J. Zimmermann, Phys. Rev. **140**, A490 (1965).

[29]See, for example, F. Nickel, D. Marx, K. Güttner, S. Hofmann, and G. Münzenberg, Z. Phys. A **288**, 125 (1978).

[30]F. M. Kiely and B. D. Pate, Nucl. Instrum. Methods **109**, 335 (1973).

[31]W. E. Frahn, Ann. Phys. (N.Y.) **72**, 524 (1972).

[32]J. R. Birkelund, J. R. Huizenga, H. Freiesleben, K. L. Wolf, J. P. Unik, and V. E. Viola, Jr., Phys. Rev. C **13**, 133 (1976).

[33]J. V. Kratz, A. E. Norris, and G. T. Seaborg, Phys. Rev. Lett. **33**, 502 (1974).